
Kinematics of the Galaxy from a Sample of Young Open Star Clusters with Data from the Gaia DR2 Catalogue

V.V. Bobylev¹ and A.T. Bajkova

*Pulkovo Astronomical Observatory, Russian Academy of Sciences,
Pulkovskoe sh. 65, St. Petersburg, 196140 Russia*

Abstract—We have selected a sample of 326 young ($\log t < 8$) open star clusters with the proper motions and distances calculated by various authors from Gaia DR2 data. The mean values of their line-of-sight velocities have also been taken from various publications. As a result of our kinematic analysis, we have found the following parameters of the angular velocity of Galactic rotation: $\Omega_0 = 29.34 \pm 0.31 \text{ km s}^{-1} \text{ kpc}^{-1}$, $\Omega'_0 = -4.012 \pm 0.074 \text{ km s}^{-1} \text{ kpc}^{-2}$, and $\Omega''_0 = 0.779 \pm 0.062 \text{ km s}^{-1} \text{ kpc}^{-3}$. The circular rotation velocity of the solar neighborhood around the Galactic center is $V_0 = 235 \pm 5 \text{ km s}^{-1}$ for the adopted Galactocentric distance of the Sun $R_0 = 8.0 \pm 0.15 \text{ kpc}$. The amplitudes of the tangential and radial velocity perturbations produced by the spiral density wave are $f_\theta = 3.8 \pm 1.2 \text{ km s}^{-1}$ and $f_R = 4.7 \pm 1.0 \text{ km s}^{-1}$, respectively; the perturbation wavelengths are $\lambda_\theta = 2.3 \pm 0.5 \text{ kpc}$ and $\lambda_R = 2.2 \pm 0.5 \text{ kpc}$ for the adopted four-armed spiral pattern. The Sun's phase in the spiral density wave is close to $\chi_\odot = -120 \pm 10^\circ$.

INTRODUCTION

Open star clusters (OSCs) play an important role for studying the Galaxy and its subsystems, because the mean values of a number of kinematic and photometric parameters derived from them are highly accurate. OSCs are used as a tool for studying the properties of the Galactic thin and thick disks, their dynamical and chemical evolution, the spiral structure, the star formation processes, establishing the distance scale, etc.

The second Gaia data release (Gaia DR2) was published in April 2018 (Brown et al. 2018; Lindegren et al. 2018), while the third data release is scheduled to be issued in mid-2020. The Gaia DR2 catalogue contains the trigonometric parallaxes and proper motions of ~ 1.7 billion stars. The derivation of their values is based on the orbital observations performed for 22 months. The mean errors of the trigonometric parallax and both proper motion components in this catalogue depend on magnitude. For example, the parallax errors lie in the range 0.02–0.04 mas for bright stars ($G < 15^m$) and are 0.7 mas for faint stars ($G = 20^m$). For quite a few (more than 7 million) stars of spectral types F–G–K their line-of-sight velocities were determined with a mean error of $\sim 1 \text{ km s}^{-1}$.

Using highly accurate Gaia DR2 data has allowed one to derive new mean values of the kinematic parameters for quite a few OSCs (Babusiaux et al. 2018; Kuhn et al. 2019; Cantat-Gaudin et al. 2018), to study the spatial and intrinsic kinematic properties of a number of young stellar associations (Zari et al. 2018; Franciosini et al. 2018; Roccatagliata

¹e-mail: vbobylev@gaoran.ru

et al. 2018; Kounkel et al. 2018) and OSCs (Soubiran et al. 2018; Dias et al. 2018) close to the Sun with unprecedented detail, to detect new OSCs (Beccari et al. 2018), and to study the fine structure of the Hertzsprung–Russell diagram (Babusiaux et al. 2018) important for refining the empirical isochrones and the evolutionary processes, which must result in a deeper understanding of the physics of stars.

At relative parallax errors for stars from the Gaia DR2 catalogue less than 10% the radius of the solar neighborhood with these stars is ~ 3 kpc (Fig. 1 in Xu et al. (2018)). This allows one to cover almost the entire Local Arm and to reach the edges of the Perseus and Carina–Sagittarius arms and to determine the parameters of the spiral structure.

Previously (Bobylev and Bajkova 2018), based on a sample of ~ 500 OB stars with proper motions and parallaxes from the Gaia DR2 catalogue, we refined the Galactic rotation parameters and the parameters of the spiral density wave. One might expect that, given the necessary statistics, a kinematic analysis of OSCs using the parameters calculated from GaiaDR2 data will allow these results to be confirmed or even improved, because the velocities of OSCs are determined with a higher accuracy than are the velocities of single stars.

The goal of this paper is to refine the rotation parameters of the Galaxy and its spiral structure using the latest data on OSCs. For this purpose, we use the mean proper motions and parallaxes of OSCs calculated by various authors exclusively from Gaia DR2 data, while the mean line-of-sight velocities of these OSCs were derived mostly from ground-based observations, although there are cases where they were determined from Gaia DR2 data.

DATA

Proper Motions and Line-of-Sight Velocities of OSCs

The main source of the mean proper motions and parallaxes calculated from Gaia DR2 data for us was the paper by Cantat-Gaudin et al. (2018), where these quantities were determined for 1229 OSCs. The parameters of several more OSCs were taken from Babusiaux et al. (2018), where they were calculated exclusively from Gaia DR2 data based on a large number of most probable cluster members.

We took the mean heliocentric line-of-sight velocities of OSCs mostly from the MWSC (Milky Way Star Clusters) catalogue (Kharchenko et al. 2013) and, in several cases, from Kuhn et al. (2018), Babusiaux et al. (2018), Casamiquela et al. (2016), Conrad et al. (2014), and Mermilliod et al. (2008). Soubiran et al. (2018) showed that there is good agreement between the line-of-sight velocities of OSCs calculated only from Gaia DR2 data and those from the MWSC catalogue.

In this paper we consider OSCs with relative parallax errors $\sigma_\pi/\pi < 30\%$, where the dispersion σ_π was taken from column 109 in the catalogue by Cantat-Gaudin et al. (2018). There are 925 such OSCs of various ages for each of which there are proper motions and parallaxes. Out of them, 459 OSCs also have line-of-sight velocity estimates; for these clusters we can calculate their total space velocities. The last sample contains 211 relatively young OSCs for which $\log t < 8$. Precisely these OSCs are of greatest interest for studying the Galactic kinematics, because they belong to the rotating thin disk, are affected by the spiral density wave, and must have a low residual velocity dispersion. In this sample the relative parallax errors for all OSCs do not exceed 30%. Their distribution on the $l - -Z$ plane (l is the Galactic longitude, Z is the coordinate in a rectangular coordinate system

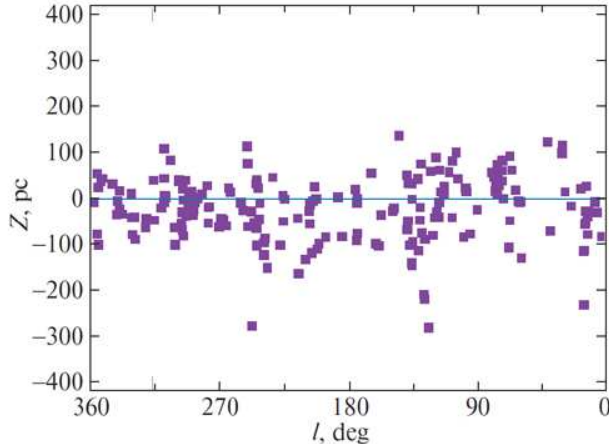


Figure 1: Positions of young ($\log t < 8$) OSCs relative to the Galactic plane.

toward the Galactic Pole) is shown in Fig. 1. As can be seen from the figure, all these OSCs are no more than 300 pc away from the Galactic plane, i.e., they all belong to the thin disk. An asymmetry in the distribution of OSCs relative to the horizontal axis is also clearly seen. This reflects the well-known fact of the Sun’s elevation above the Galactic plane. From the data on 211 OSCs we found $Z_{\odot} = -20 \pm 5$ pc. This value is in good agreement with the results of our analysis of samples of other young thin-disk objects (Bobylev and Bajkova 2016).

Correction to the Gaia DR2 Parallaxes

The presence of a possible systematic offset $\Delta\pi = -0.029$ mas in the Gaia DR2 parallaxes with respect to an inertial reference frame was first pointed out by Lindegren et al. (2018). Here the minus means that this correction should be added to the Gaia DR2 stellar parallaxes to reduce them to the standard. At present, there are several reliable distance scales a comparison with which, in the opinion of their authors, allows the systematics of the Gaia trigonometric parallaxes to be controlled. Arenou et al. (2018) compared the Gaia DR2 parallaxes with 29 independent catalogues that confirm the presence of an offset in the Gaia DR2 parallaxes $\Delta\pi \sim -0.03$ mas.

Stassun and Torres (2018) found the correction $\Delta\pi = -0.082 \pm 0.033$ mas by comparing the parallaxes of 89 detached eclipsing binaries with their trigonometric parallaxes from the Gaia DR2 catalogue. These stars were selected from published data using very rigorous criteria imposed on the photometric parameters. As a result, the relative errors in the stellar radii, effective temperatures, and bolometric luminosities, from which the distances are estimated, do not exceed 3%.

Bobylev (2019) obtained an estimate of $\Delta\pi = -0.038 \pm 0.046$ mas from a comparison of 88 radio stars whose trigonometric parallaxes were measured by various authors by means of VLBI with the Gaia DR2 catalogue. It is well known that this method allows the stellar parallaxes to be determined with an error of $\sim 10 \mu\text{as}$. However, so far there are few such stars and, therefore, the error in the estimate is great.

By comparing the astrometric (Gaia DR2) and photometric parallaxes of 94 OSCs, Yalyalieva et al. (2018) found the correction $\Delta\pi = -0.045 \pm 0.009$ mas. The high ac-

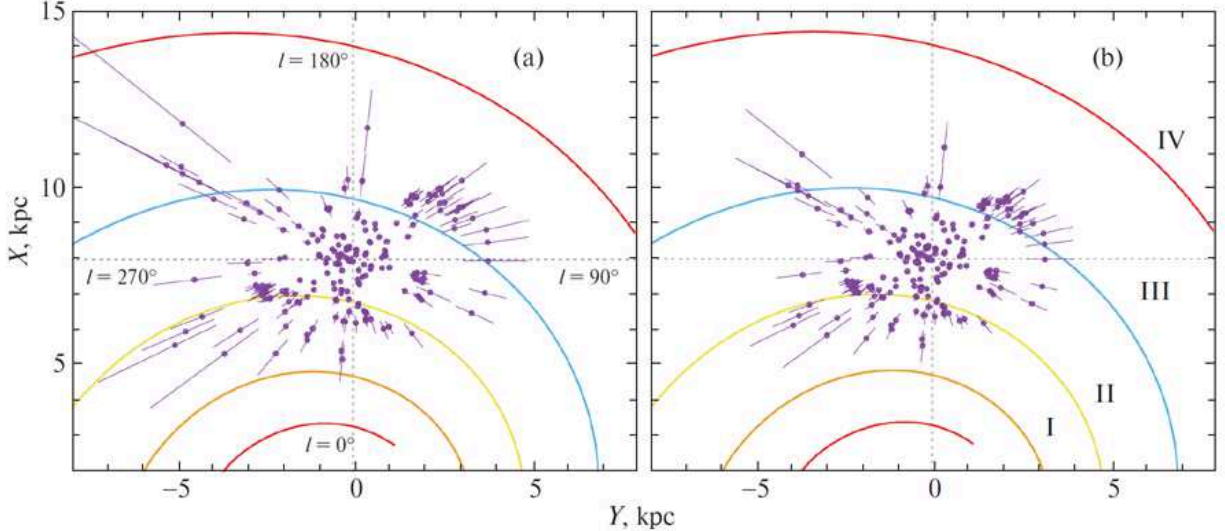


Figure 2: Distribution of young ($\log t < 8$) OSCs whose distances were calculated using the original parallaxes from the Gaia DR2 catalogue (a) and with the correction $\Delta\pi = 0.050$ mas (b) on the Galactic XY plane; The Sun has coordinates $(X, Y) = (8, 0)$ kpc, the four-armed spiral pattern with a pitch angle of -13° is shown (Bobylev and Bajkova 2014), the spiral arm segments are numbered by Roman numerals.

accuracy of this estimate is related to the high accuracy of photometric distance estimates for OSCs. The data from up-to-date first-class infrared photometric surveys, such as IPHAS, 2MASS, WISE, and Pan-STARRS, were invoked for this purpose.

Riess et al. (2018) obtained an estimate of $\Delta\pi = -0.046 \pm 0.013$ mas based on a sample of 50 long-period Cepheids when comparing their parallaxes with those from the Gaia DR2 catalogue. The photometric parameters of these Cepheids measured from the Hubble Space Telescope were used.

By comparing the distances of ~ 3000 stars from the APOKAS-2 catalogue (Pinsonneault et al. 2018) belonging to the red giant branch with the Gaia DR2 data, Zinn et al. (2018) found the correction $\Delta\pi = -0.053 \pm 0.003$ mas. These authors also obtained a close value by analyzing stars belonging to the so called red clump, $\Delta\pi = -0.050 \pm 0.004$ mas. The distances to such stars were estimated from asteroseismic data. According to these authors, the parallax errors here are approximately equal to the errors in estimating the stellar radius and are, on average, 1.5%. Such small errors in combination with the enormous number of stars allowed $\Delta\pi$ to be determined with a high accuracy.

Note also the experiment to compare the distances to OSCs from various catalogues described in Cantat-Gaudin et al. (2018). It showed that the correction $\Delta\pi$ differs from that recommended by Lindegren et al. (2018) and should be close to -0.050 mas.

The listed results lead to the conclusion that the trigonometric parallaxes of stars from the Gaia DR2 catalogue should be corrected by applying a small correction. We will be oriented to the results of Yalyalieva et al. (2018), Riess et al. (2018), and Zinn et al. (2018), which look most reliable.

Note that two types of distances are given in the catalogue by Cantat-Gaudin et al. (2018). First, it gives the mean parallaxes of OSCs calculated from the original trigonometric parallaxes of probable cluster members that were taken by these authors from the Gaia DR2

catalogue. In this paper we use precisely these values (and similar values taken from other authors) to calculate the distances to OSCs. Second, it gives the distances to OSCs calculated from the mean parallaxes by adding the correction $\Delta\pi = 0.029$ mas, but these distances are not used here.

Figure 2 shows the distribution of young OSCs whose distances were calculated both using the original mean parallaxes from the Gaia DR2 catalogue and by adding the correction $\Delta\pi = 0.050$ mas to these values on the Galactic XY plane. The Roman numerals in the figure number the following spiral arm segments: Scutum (I), Carina–Sagittarius (II), Perseus (III), and the Outer Arm (IV). It follows from the figure that the correction affects significantly the distance calculations for OSCs, especially those far from the Sun. Note also that the distribution of points in Fig. 2b agrees better with the above spiral pattern.

METHOD

We know three stellar velocity components from observations: the line-of-sight velocity V_r and the two tangential velocity components $V_l = 4.74r\mu_l \cos b$ and $V_b = 4.74r\mu_b$ along the Galactic longitude l and latitude b , respectively, expressed in km s^{-1} . Here, the coefficient 4.74 is the ratio of the number of kilometers in an astronomical unit to the number of seconds in a tropical year, and $r = 1/\pi$ is the stellar heliocentric distance in kpc. The proper motion components $\mu_l \cos b$ and μ_b are expressed in mas yr^{-1} . The velocities U, V, W directed along the rectangular Galactic coordinate axes are calculated via the components V_r, V_l, V_b :

$$\begin{aligned} U &= V_r \cos l \cos b - V_l \sin l - V_b \cos l \sin b, \\ V &= V_r \sin l \cos b + V_l \cos l - V_b \sin l \sin b, \\ W &= V_r \sin b + V_b \cos b, \end{aligned} \tag{1}$$

where the velocity U is directed from the Sun toward the Galactic center, V is in the direction of Galactic rotation, and W is directed to the north Galactic pole. We can find two velocities, V_R directed radially away from the Galactic center and the velocity V_{circ} orthogonal to it pointing in the direction of Galactic rotation, based on the following relations:

$$\begin{aligned} V_{circ} &= U \sin \theta + (V_0 + V) \cos \theta, \\ V_R &= -U \cos \theta + (V_0 + V) \sin \theta, \end{aligned} \tag{2}$$

where the position angle θ obeys the relation $\tan \theta = y/(R_0 - x)$, and x, y, z are the rectangular heliocentric coordinates of the star (the velocities U, V, W are directed along the corresponding x, y, z axes), V_0 is the linear rotation velocity of the Galaxy at the solar distance R_0 . The velocities V_R and W are virtually independent of the pattern of the Galactic rotation curve. However, to analyze the periodicities in the tangential velocities, it is necessary to determine a smoothed Galactic rotation curve and to form the residual velocities ΔV_{circ} .

To determine the parameters of the Galactic rotation curve, we use the equations derived from Bottlinger's formulas, in which the angular velocity Ω is expanded into a series to terms of the second order of smallness in r/R_0 :

$$\begin{aligned} V_r &= -U_\odot \cos b \cos l - V_\odot \cos b \sin l - W_\odot \sin b \\ &+ R_0(R - R_0) \sin l \cos b \Omega'_0 + 0.5R_0(R - R_0)^2 \sin l \cos b \Omega''_0, \end{aligned} \tag{3}$$

$$V_l = U_\odot \sin l - V_\odot \cos l - r\Omega_0 \cos b \\ + (R - R_0)(R_0 \cos l - r \cos b)\Omega'_0 + 0.5(R - R_0)^2(R_0 \cos l - r \cos b)\Omega''_0, \quad (4)$$

$$V_b = U_\odot \cos l \sin b + V_\odot \sin l \sin b - W_\odot \cos b \\ - R_0(R - R_0) \sin l \sin b \Omega'_0 - 0.5R_0(R - R_0)^2 \sin l \sin b \Omega''_0, \quad (5)$$

where R is the distance from the star to the Galactic rotation axis:

$$R^2 = r^2 \cos^2 b - 2R_0 r \cos b \cos l + R_0^2. \quad (6)$$

The quantity Ω_0 is the angular velocity of Galactic rotation at the solar distance R_0 , the parameters Ω'_0 and Ω''_0 are the corresponding derivatives of the angular velocity, and $V_0 = |R_0\Omega_0|$. As experience shows, to construct a smooth Galactic rotation curve in the range of distances R from 2 to 12 kpc, it will suffice to know two derivatives of the angular velocity, Ω'_0 and Ω''_0 . Note that the velocities V_R and ΔV_{circ} must be freed from the peculiar solar velocity $U_\odot, V_\odot, W_\odot$.

A number of studies devoted to determining the mean distance from the Sun to the Galactic center using its individual determinations in the last decade by independent methods have been performed by now. For example, $R_0 = 8.0 \pm 0.2$ kpc (Vallée 2017a), $R_0 = 8.4 \pm 0.4$ kpc (de Grijs and Bono 2017), or $R_0 = 8.0 \pm 0.15$ kpc (Camarillo et al. 2018). Based on these reviews, in this paper we adopted $R_0 = 8.0 \pm 0.15$ kpc.

The influence of the spiral density wave in the radial (V_R) and residual tangential (ΔV_{circ}) velocities is periodic with an amplitude of $\sim 6\text{--}10$ km s $^{-1}$. According to the linear theory of density waves (Lin and Shu 1964), it is described by the following relations:

$$V_R = -f_R \cos \chi, \\ \Delta V_{circ} = f_\theta \sin \chi, \quad (7)$$

where

$$\chi = m[\cot(i) \ln(R/R_0) - \theta] + \chi_\odot \quad (8)$$

is the phase of the spiral density wave (m is the number of spiral arms, i is the pitch angle of the spiral pattern, and χ_\odot is the Sun's radial phase in the spiral density wave); f_R and f_θ are the amplitudes of the radial and tangential velocity perturbations, which are assumed to be positive. As an analysis of the present day highly accurate data showed, the periodicities associated with the spiral density wave also manifest themselves in the vertical velocities W (Bobilev and Bajkova 2015; Rastorguev et al. 2017).

We apply a modified spectral analysis (Bajkova and Bobilev 2012) to study the periodicities in the velocities V_R and ΔV_{circ} . The wavelength λ (the distance between adjacent spiral arm segments measured along the radial direction) is calculated from the relation

$$\frac{2\pi R_0}{\lambda} = m \cot(i). \quad (9)$$

Let there be a series of measured velocities V_{R_n} (these can be both radial (V_R) and tangential (ΔV_{circ}) velocities), $n = 1, \dots, N$, where N is the number of objects. The objective of our spectral analysis is to extract a periodicity from the data series in accordance with the adopted model describing a spiral density wave with parameters f , λ (or i) and χ_\odot .

Having taken into account the logarithmic behavior of the spiral density wave and the position angles of the objects θ_n , our spectral (periodogram) analysis of the series of velocity

perturbations is reduced to calculating the square of the amplitude (power spectrum) of the standard Fourier transform (Bajkova and Bobylev 2012):

$$\bar{V}_{\lambda_k} = \frac{1}{N} \sum_{n=1}^N V'_n(R'_n) \exp\left(-j \frac{2\pi R'_n}{\lambda_k}\right), \quad (10)$$

where \bar{V}_{λ_k} is the k th harmonic of the Fourier transform with wavelength $\lambda_k = D/k$, D is the period of the series being analyzed,

$$\begin{aligned} R'_n &= R_0 \ln(R_n/R_0), \\ V'_n(R'_n) &= V_n(R'_n) \times \exp(jm\theta_n). \end{aligned} \quad (11)$$

The sought-for wavelength λ corresponds to the peak value of the power spectrum S_{peak} . The pitch angle of the spiral density wave is derived from Eq. (9). We determine the perturbation amplitude and phase by fitting the harmonic with the wavelength found to the observational data. The following relation can also be used to estimate the perturbation amplitude:

$$f_R(f_\theta) = 2 \times \sqrt{S_{peak}}. \quad (12)$$

Thus, our approach consists of two steps: (i) the construction of a smooth Galactic rotation curve and (ii) a spectral analysis of the radial (V_R) and residual tangential (ΔV_{circ}) velocities. This method was applied by Bobylev and Bajkova (2012, 2013, 2015, 2018) to study the kinematics of young Galactic objects.

Monte Carlo Simulations

We use Monte Carlo simulations to estimate the errors in the parameters of the spiral density wave being determined. In accordance with this method, we generate M independent realizations of data on the parallaxes and velocities of objects with their random measurement errors that are known to us.

We assume that the measurement errors of the data are distributed normally with a mean equal to the nominal value and a dispersion equal to $\sigma_l = error_l$, $l = 1, \dots, N_d$, where N_d is the number of data and $error_l$ denotes the measurement error of a single measurement with number l (one sigma). Each element of a random realization is formed independently by adding the nominal value of the measured data with number l and the random number generated according to a normal law with zero mean and dispersion σ_l . Note that the latter is limited from above by $3\sigma_l$.

Each random realization of data with number j ($j = 1, \dots, M$) generated in this way is then processed according to the algorithm described above to determine the sought-for parameters $f_R^j, \lambda^j, \chi_\odot^j$. The mean values of the parameters and their dispersions are then determined from the derived sequences of estimates: $m_{f_R} \pm \sigma_{f_R}, m_\lambda \pm \sigma_\lambda, m_{\chi_\odot} \pm \sigma_{\chi_\odot}$. The statistical parameters of the spiral density wave pitch angle i can be determined using Eq. (9): $m_i \pm \sigma_i$.

RESULTS

The system of conditional equations (3)–(5) is solved by the least-squares method with weights of the form $w_r = S_0/\sqrt{S_0^2 + \sigma_{V_r}^2}$, $w_l = S_0/\sqrt{S_0^2 + \sigma_{V_l}^2}$ and $w_b = S_0/\sqrt{S_0^2 + \sigma_{V_b}^2}$, where

S_0 is the “cosmic” dispersion, $\sigma_{V_r}, \sigma_{V_l}, \sigma_{V_b}$ are the dispersions of the corresponding observed velocities. S_0 is comparable to the root-mean-square residual σ_0 (the error per unit weight) in solving the conditional equations (3)–(5). We adopted $S_0 = 8 \text{ km s}^{-1}$ when analyzing the sample of young OSCs and $S_0 = 11 \text{ km s}^{-1}$ for the sample of older OSCs. The system of equations (3)–(5) was solved in several iterations using the 3σ criterion to eliminate the OSCs with large residuals.

Method I. The first method consists in seeking a solution based on such OSCs for which the space velocities U, V, W can be calculated. First, based on the sample of 211 relatively young ($\log t < 8$) OSCs, we obtained a solution of the system of conditional equations (3)–(5) from the original data, i.e., without correcting the parallaxes. The following kinematic parameters were found in this approach:

$$\begin{aligned} (U_\odot, V_\odot, W_\odot) &= (7.63, 11.72, 8.93) \pm (0.60, 0.74, 0.61) \text{ km s}^{-1}, \\ \Omega_0 &= 28.34 \pm 0.37 \text{ km s}^{-1} \text{ kpc}^{-1}, \\ \Omega'_0 &= -3.832 \pm 0.090 \text{ km s}^{-1} \text{ kpc}^{-2}, \\ \Omega''_0 &= 0.851 \pm 0.073 \text{ km s}^{-1} \text{ kpc}^{-3}. \end{aligned} \tag{13}$$

In this solution the error per unit weight is $\sigma_0 = 8.5 \text{ km s}^{-1}$.

The next solution of the conditional equations (3)–(5) was obtained with the corrected OSC parallaxes by applying the correction $\Delta\pi = 0.050 \text{ mas}$. In this case, the following kinematic parameters were found:

$$\begin{aligned} (U_\odot, V_\odot, W_\odot) &= (7.36, 12.15, 8.22) \pm (0.57, 0.72, 0.57) \text{ km s}^{-1}, \\ \Omega_0 &= 28.79 \pm 0.39 \text{ km s}^{-1} \text{ kpc}^{-1}, \\ \Omega'_0 &= -3.999 \pm 0.091 \text{ km s}^{-1} \text{ kpc}^{-2}, \\ \Omega''_0 &= 0.921 \pm 0.096 \text{ km s}^{-1} \text{ kpc}^{-3}. \end{aligned} \tag{14}$$

In this solution the error per unit weight is $\sigma_0 = 7.9 \text{ km s}^{-1}$. For the adopted $R_0 = 8.0 \pm 0.15 \text{ kpc}$ the linear Galactic rotation velocity ($V_0 = |R_0\Omega_0|$) is $V_0 = 230 \pm 6 \text{ km s}^{-1}$, while the Oort constants ($A = -0.5\Omega'_0 R_0$ and $B = \Omega_0 + A$) take the following values: $A = 16.00 \pm 0.37 \text{ km s}^{-1} \text{ kpc}^{-1}$ and $B = -12.79 \pm 0.53 \text{ km s}^{-1} \text{ kpc}^{-1}$.

Method II. In this approach we exploit all potentialities of the available data. The clusters with the proper motions, line-of-sight velocities, and distances give all three equations (3)–(5), while the clusters for which only the proper motions are available give only two equations, (4) and (5). We solve this system of equations simultaneously.

We apply this method to analyze OSCs younger than 1 Gyr ($\log t < 9$). For this purpose, we divided the sample into two parts: 326 relatively young ($\log t < 8$) OSCs and 481 older ($8 < \log t < 9$) OSCs.

Based on the sample of young ($\log t < 8$) OSCs, we found the following kinematic parameters:

$$\begin{aligned} (U_\odot, V_\odot, W_\odot) &= (7.88, 11.17, 8.28) \pm (0.48, 0.63, 0.45) \text{ km s}^{-1}, \\ \Omega_0 &= 29.34 \pm 0.31 \text{ km s}^{-1} \text{ kpc}^{-1}, \\ \Omega'_0 &= -4.012 \pm 0.074 \text{ km s}^{-1} \text{ kpc}^{-2}, \\ \Omega''_0 &= 0.779 \pm 0.062 \text{ km s}^{-1} \text{ kpc}^{-3}, \end{aligned} \tag{15}$$

where the error per unit weight is $\sigma_0 = 7.9 \text{ km s}^{-1}$, the Galactic rotation velocity is $V_0 = 235 \pm 5 \text{ km s}^{-1}$, and the Oort constants are $A = 16.05 \pm 0.30 \text{ km s}^{-1} \text{ kpc}^{-1}$ and $B = -13.29 \pm 0.43 \text{ km s}^{-1} \text{ kpc}^{-1}$. Basically, this solution is an improvement of the solution (14), because 115

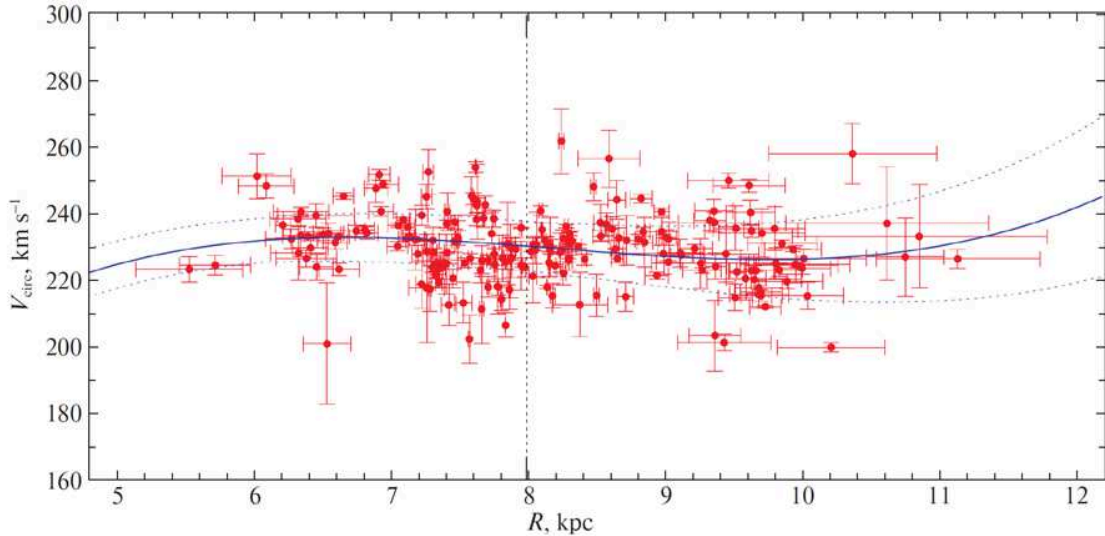


Figure 3: Circular velocities of young OSCs versus Galactocentric distance. The Galactic rotation curve constructed according to the solution (14) with 1σ confidence intervals is presented; the vertical dotted line marks the Sun's position.

more OSCs for which only the parallaxes and proper motions are available were added here to the 211 OSCs used in seeking the solution (14).

Based on the sample of 481 older ($8 < \log t < 9$) OSCs, we found the following kinematic parameters:

$$\begin{aligned}
 (U_{\odot}, V_{\odot}, W_{\odot}) &= (8.58, 11.10, 7.54) \pm (0.61, 0.76, 0.52) \text{ km s}^{-1}, \\
 \Omega_0 &= 28.42 \pm 0.39 \text{ km s}^{-1} \text{ kpc}^{-1}, \\
 \Omega'_0 &= -3.972 \pm 0.097 \text{ km s}^{-1} \text{ kpc}^{-2}, \\
 \Omega''_0 &= 0.642 \pm 0.061 \text{ km s}^{-1} \text{ kpc}^{-3},
 \end{aligned}
 \tag{16}$$

where the error per unit weight is $\sigma_0 = 11.1 \text{ km s}^{-1}$, the Galactic rotation velocity is $V_0 = 227 \pm 5 \text{ km s}^{-1}$, and the Oort constants are $A = 15.89 \pm 0.39 \text{ km s}^{-1} \text{ kpc}^{-1}$ and $B = -12.54 \pm 0.55 \text{ km s}^{-1} \text{ kpc}^{-1}$.

Velocity Perturbations from the Density Wave

In Fig 3 the circular velocities of OSCs are plotted against the Galactocentric distance; the Galactic rotation curve constructed according to the solution (15) is presented. As can be seen from the figure, the residual velocities have a low dispersion; a periodicity with a length of about 2 kpc is clearly visible.

Based on the deviation from the Galactic rotation curve (15), we calculated the residual circular velocities ΔV_{circ} . Based on the series of radial (V_R) and residual tangential (ΔV_{circ}) velocities for this sample of OSCs, we found the parameters of the Galactic spiral density wave by applying a periodogram analysis. The amplitudes of the radial and tangential velocity perturbations are $f_R = 4.7 \pm 1.0 \text{ km s}^{-1}$ and $f_{\theta} = 3.8 \pm 1.2 \text{ km s}^{-1}$, respectively.

Figure 4 shows the power spectra of the OSC velocities. It is clearly seen from this figure that the peaks of the distribution lie almost at the same λ in both cases. Indeed, the

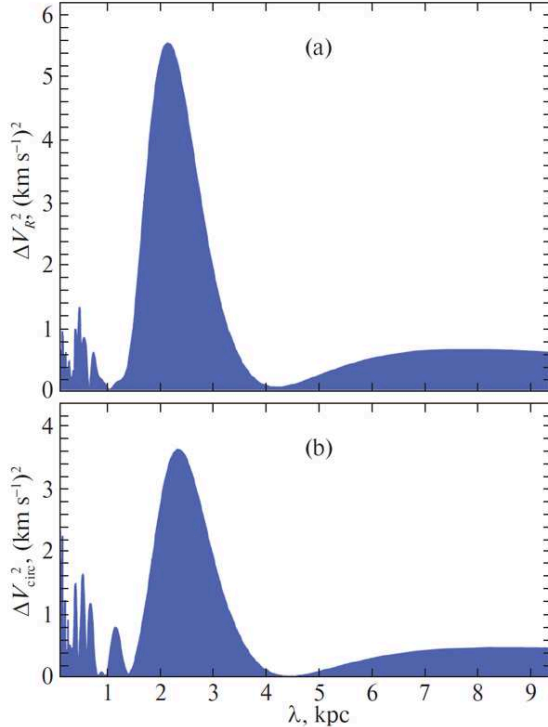


Figure 4: Power spectra of the radial (a) and residual tangential (b) velocities for young OSCs.

perturbation wavelengths are $\lambda_R = 2.2 \pm 0.5$ kpc ($i = -10 \pm 2^\circ$) and $\lambda_\theta = 2.3 \pm 0.5$ kpc ($i = -11 \pm 2^\circ$) for the adopted four-armed spiral pattern ($m = 4$).

Figure 5 presents the radial and residual tangential velocities of OSCs. It is clearly seen that the periodic curves in Figs. 5a and 5b go with a phase shift of 90° . We measure the Sun’s phase in the spiral density wave χ_\odot from the Carina–Sagittarius arm ($R \sim 7$ kpc); in our case, its value is very close to $-120 \pm 10^\circ$.

A number of OSCs that deviate significantly from the overall pattern can be seen in Figs. 3 and 5. For example, the cluster Stock 16 ($R = 6.5$ kpc) has a large deviation from the rotation curve, $\Delta V_{circ} = -32 \pm 18$ km s $^{-1}$. One more OSC that does not “march in step”, NGC 2453 ($R = 10.4$ kpc), has $\Delta V_{circ} = 31 \pm 9$ km s $^{-1}$. Both these clusters have large relative parallax errors, $\sigma_\pi/\pi = 30\%$ for Stock 16 and $\sigma_\pi/\pi = 22\%$ for NGC 2453. Whereas Stock 16 is fairly young, $\log t = 6.78$, NGC 2453 is older, $\log t = 7.86$. Note that both these clusters and several more OSCs with smaller random errors in the velocities V_R and V_{circ} were rejected according to the 3σ criterion when seeking the solutions (13)–(15).

DISCUSSION

Bobylev et al. (2016) performed a kinematic analysis of OSCs from the MWSC catalogue (Kharchenko et al. 2013) using photometric distance estimates. First of all, it should be noted that the distribution of the sample of young OSCs with trigonometric parallaxes on the Galactic XY plane (Fig. 2) visually agrees much better with the model of a spiral pattern than does their distribution that was derived using photometric distance estimates

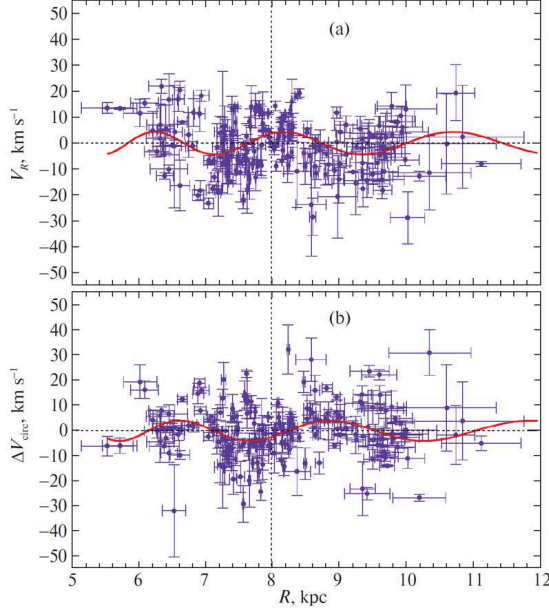


Figure 5: Radial (a) and residual tangential (b) velocities of young OSCs versus Galactocentric distance; the vertical dotted line marks the Sun’s position.

(see Fig. 1 in Bobylev et al. (2016)).

The error per unit weight σ_0 that we find when solving the conditional equations (3)–(5) characterizes the residual velocity dispersion for OSCs averaged over three directions. The residual velocity dispersion for hydrogen clouds in the Galactic disk is known to be ~ 5 km s $^{-1}$. The residual velocity dispersion for OB stars lies in the range 8–10 km s $^{-1}$; the analogous velocity dispersion for Cepheids is ~ 14 km s $^{-1}$. One might expect the velocity dispersion for young OSCs to be close to that for OB stars. In the solutions (14) and (15) we found $\sigma_0 = 7.9$ km s $^{-1}$, which agrees excellently with the expected value. Therefore, it is surprising that when analyzing the youngest OSCs from the MWSC catalogue (Kharchenko et al. 2013), σ_0 is 15.7 km s $^{-1}$ in Bobylev et al. (2016). This can be explained by the fact that the errors of the stellar proper motions taken from the PPMXL catalogue (Röser et al. 2010), where their values lie in the range 4–10 mas yr $^{-1}$, i.e., exceed the random errors of the Gaia DR2 stellar proper motions by two orders of magnitude, are great. The errors of the photometric distances also make their contribution.

The results of the solution (16) are also of indubitable interest. The increase in σ_0 to 11.1 km s $^{-1}$ is related to the growth of the velocity dispersions with increasing stellar age (disk heating), with the contribution of the purely measurement errors being negligible here. For example, for OSCs with a close age Bobylev et al. (2016) found $\sigma_0 = 21$ km s $^{-1}$.

Based on a sample of 209 young ($\log t < 7.7$) OSCs from the MWSC catalogue, Bobylev et al. (2016) found the following solar velocity components: $(U_\odot, V_\odot, W_\odot) = (9.7, 11.2, 6.2) \pm (1.1, 1.4, 1.1)$ km s $^{-1}$ and parameters of the Galactic rotation curve: $\Omega_0 = 28.60 \pm 0.81$ km s $^{-1}$ kpc $^{-1}$, $\Omega'_0 = -4.04 \pm 0.16$ km s $^{-1}$ kpc $^{-2}$ and $\Omega''_0 = 0.19 \pm 0.13$ km s $^{-1}$ kpc $^{-3}$ ($R_0 = 8.3 \pm 0.2$ kpc was adopted). We can see that in the solution (14), at the same number of OSCs, the errors in the parameters being determined are smaller approximately by a factor of 2.

Thus, in this paper we used virtually the same line-of-sight velocities of OSCs as those in Bobylev et al. (2016), but completely different distances and proper motions of OSCs. As a

result, we obtained reliable (σ_0 is small), new Galactic parameters in the solutions (14) and (15).

Having analyzed the proper motions and parallaxes for a local sample of 304267 main-sequence stars for the Gaia DR1 catalogue, Bovy (2017) obtained the following Oort parameters: $A = 15.3 \pm 0.5 \text{ km s}^{-1} \text{ kpc}^{-1}$ and $B = -11.9 \pm 0.4 \text{ km s}^{-1} \text{ kpc}^{-1}$, based on which he estimated the angular velocity of Galactic rotation $\Omega_0 = 27.1 \pm 0.5 \text{ km s}^{-1} \text{ kpc}^{-1}$ and the corresponding linear velocity $V_0 = 219 \pm 4 \text{ km s}^{-1}$.

Based on 130 masers with measured VLBI trigonometric parallaxes, Rastorguev et al. (2017) found the solar velocity components $(U_\odot, V_\odot) = (11.40, 17.23) \pm (1.33, 1.09) \text{ km s}^{-1}$ and the following parameters of the Galactic rotation curve: $\Omega_0 = 28.93 \pm 0.53 \text{ km s}^{-1} \text{ kpc}^{-1}$, $\Omega'_0 = -3.96 \pm 0.07 \text{ km s}^{-1} \text{ kpc}^{-2}$, $\Omega''_0 = 0.87 \pm 0.03 \text{ km s}^{-1} \text{ kpc}^{-3}$ and $V_0 = 243 \pm 10 \text{ km s}^{-1}$ (for $R_0 = 8.40 \pm 0.12 \text{ kpc}$ found).

Based on a sample of 495 OB stars with proper motions from the Gaia DR2 catalogue, Bobylev and Bajkova (2018) found the following kinematic parameters: $(U, V, W)_\odot = (8.16, 11.19, 8.55) \pm (0.48, 0.56, 0.48) \text{ km s}^{-1}$, $\Omega_0 = 28.92 \pm 0.39 \text{ km s}^{-1} \text{ kpc}^{-1}$, $\Omega'_0 = -4.087 \pm 0.083 \text{ km s}^{-1} \text{ kpc}^{-2}$, $\Omega''_0 = 0.703 \pm 0.067 \text{ km s}^{-1} \text{ kpc}^{-3}$ and $V_0 = 231 \pm 5 \text{ km s}^{-1}$ (for the adopted $R_0 = 8.0 \pm 0.15 \text{ kpc}$). We conclude that the kinematic parameters found in the solutions (14) and (15) are in good agreement with the results of an analysis of the present-day data obtained by Bovy (2017), Rastorguev et al. (2017), and Bobylev and Bajkova (2018). Judging by the level of random errors in the parameters being determined, the solution (15) is one of the best at present. It is slightly inferior in parameter Ω''_0 (a large radius of the neighborhood is required here) only to the solution obtained by Rastorguev et al. (2017) based on a sample of masers with VLBI parallaxes.

The parameters of the spiral density wave. The mean pitch angle of the global four-armed spiral pattern in our Galaxy $i = -13.6 \pm 0.4^\circ$ is given in the review by Vallée (1917b). Then, for $m = 4$ and $R_0 = 8.0 \text{ kpc}$ $\lambda = 3.0 \text{ kpc}$ follows from Eq. (9). We can see that the analysis of our sample of young OSCs gives a lower value of λ and, accordingly, a smaller pitch angle $|i| : 10 - 11^\circ$.

Having analyzed the spatial distribution of a large sample of classical Cepheids, Dambis et al. (2015) estimated the pitch angle of the spiral pattern, $i = -9.5^\circ \pm 0.1^\circ$, and the Sun's phase, $\chi_\odot = -121^\circ \pm 3^\circ$, for the four-armed spiral pattern.

On the other hand, having analyzed maser sources with VLBI parallaxes, Rastorguev et al. (2017) found $i = -10.4^\circ \pm 0.3^\circ$ and $\chi_\odot = -125^\circ \pm 10^\circ$, which is in good agreement with our results. The amplitude of the radial velocity perturbations f_R is typically $6-10 \text{ km s}^{-1}$ from masers (Rastorguev et al. 2017), OB stars (Bobylev and Bajkova 2015, 2018), or Cepheids (Bobylev and Bajkova 2012). For a more reliable determination of the spiral density wave parameters, it is necessary to expand the OSC sample to cover a larger region of the Galaxy.

CONCLUSIONS

Thus, based on published data, we selected a sample of OSCs with proper motions and parallaxes from the Gaia DR2 catalogue. The catalogue by Cantat-Gaudin et al. (2018) served as a basis for this purpose. The MWSC catalogue (Kharchenko et al. 2013) served as the main source of line-of-sight velocities; for several OSCs the line-of-sight velocities were taken from the Gaia DR2 catalogue. This sample includes a total of 925 OSCs of various

ages with relative parallax errors less than 30%.

The sample of 326 youngest OSCs with an age $\log t < 8$ was studied in detail. All these clusters are no farther than 5 kpc away from the Sun and no higher than 300 pc above the Galactic plane. They were used to redetermine the Galactic rotation parameters and the parameters of the spiral density wave.

Following the latest results of an analysis of the zero point for the Gaia DR2 distance scale, we calculated the distances to OSCs by adding the correction $\Delta\pi = 0.050$ mas to the original mean values of their parallaxes.

As a result, we found the following parameters of the angular velocity of Galactic rotation: $\Omega_0 = 29.34 \pm 0.31$ km s⁻¹ kpc⁻¹, $\Omega'_0 = -4.012 \pm 0.074$ km s⁻¹ kpc⁻² and $\Omega''_0 = 0.779 \pm 0.062$ km s⁻¹ kpc⁻³; here the circular rotation velocity of the solar neighborhood around the Galactic center is $V_0 = 235 \pm 5$ km s⁻¹ for the adopted distance $R_0 = 8.0 \pm 0.15$ kpc.

The influence of the Galactic spiral density wave was detected both in the spatial distribution and in the velocities of the sample under study. A spectral analysis of the radial and residual tangential velocities for young OSCs showed excellent agreement in the perturbation wavelengths found independently for each type of velocities, $\lambda_R = 2.2 \pm 0.5$ kpc and $\lambda_\theta = 2.3 \pm 0.5$ kpc. For the four-armed spiral pattern ($m = 4$ and the adopted R_0) a pitch angle $i \sim -10^\circ$ corresponds to these values. The Sun's phase in the spiral density wave is close to $\chi_\odot = -120^\circ \pm 10^\circ$. The amplitudes of the radial and tangential velocity perturbations are $f_R = 4.7 \pm 1.0$ km s⁻¹ and $f_\theta = 3.8 \pm 1.2$ km s⁻¹, respectively.

We also considered a sample of 481 older ($\log t : 8 - 9$) OSCs. These OSCs were shown to rotate more slowly, with a velocity $V_0 = 227 \pm 5$ km s⁻¹. The parameters of the spiral density wave were not determined for this sample.

ACKNOWLEDGMENTS

We are grateful to the referees for their useful remarks that contributed to an improvement of the paper. This work was supported in part by Basic Research Program P-28 of the Presidium of the Russian Academy of Sciences, the subprogram ‘‘Cosmos: Studies of Fundamental Processes and their Interrelations’’.

REFERENCES

1. F. Arenou, X. Luri, C. Babusiaux, C. Fabricius, A. Helmi, T. Muraveva, A. C. Robin, F. Spoto, et al. (Gaia Collab.), *Astron. Astrophys.* 616, 17 (2018).
2. C. Babusiaux, F. van Leeuwen, M. A. Barstow, C. Jordi, A. Vallenari, A. Bossini, A. Bressan, T. Cantat-Gaudin, et al. (Gaia Collab.), *Astron. Astrophys.* 616, 10 (2018).
3. A. T. Bajkova and V. V. Bobylev, *Astron. Lett.* 38, 549 (2012).
4. G. Beccari, H. M. J. Boffin, T. Jerabkova, N. J. Wright, V. M. Kalari, G. Carraro, G. De Marchi, and W.-J. de Wit, *Mon. Not. R. Astron. Soc.* 481, L11 (2018).
5. V. V. Bobylev and A. T. Bajkova, *Astron. Lett.* 38, 638 (2012).
6. V. V. Bobylev and A. T. Bajkova, *Astron. Lett.* 39, 532 (2013).
7. V. V. Bobylev and A. T. Bajkova, *Mon. Not. R. Astron. Soc.* 437, 1549 (2014).
8. V. V. Bobylev and A. T. Bajkova, *Astron. Lett.* 41, 473 (2015).
9. V. V. Bobylev and A. T. Bajkova, *Astron. Lett.* 42, 1 (2016).
10. V. V. Bobylev, A. T. Bajkova, and K. S. Shirokova, *Astron. Lett.* 42, 721 (2016).
11. V. V. Bobylev and A. T. Bajkova, *Astron. Lett.* 44, 675 (2018).
12. V. V. Bobylev, *Astron. Lett.* 45, 10 (2019).

13. J. Bovy, *Mon. Not. R. Astron. Soc.* 468, L63 (2017).
14. A. G. A. Brown, A. Vallenari, T. Prusti, de Bruijne, C. Babusiaux, C. A. L. Bailer-Jones, M. Biermann, D.W. Evans, et al. (Gaia Collab.), *Astron. Astrophys.* 616, 1 (2018).
15. T. Camarillo, M. Varun, M. Tyler, and R. Bharat, *Publ. Astron. Soc. Pacif.* 130, 4101 (2018).
16. T. Cantat-Gaudin, C. Jordi, A. Vallenari, A. Bragaglia, L. Balaguer-Nuñez, C. Soubiran, et al., *Astron. Astrophys.* **618**, 93 (2018).
17. L. Casamiquela, R. Carrera, C. Jordi, L. Balaguer-Nuñez, E. Pancino, S. L. Hidalgo, C. E. Martínez-Vazquez, S. Murabito, et al., *Mon. Not. R. Astron. Soc.* 458, 3150 (2016).
18. C. Conrad, R.-D. Scholz, N. V. Kharchenko, A. E. Piskunov, E. Schilbach, S. Röser, C. Boeche, G. Kordopatis, et al., *Astron. Astrophys.* 562, 54 (2014).
19. A. K. Dambis, L. N. Berdnikov, Yu. N. Efremov, A. Yu. Kniazev, A. S. Rastorguev, E. V. Glushkova, V. V. Kravtsov, D. G. Turner, D. J. Majaess, and R. Sefako, *Astron. Lett.* 41, 489 (2015).
20. W. S. Dias, H. Monteiro, J. R. D. Lépine, R. Prates, C. D. Gneiding, and M. Sacchi, *Mon. Not. R. Astron. Soc.* 481, 3887 (2018).
21. E. Franciosini, G. G. Sacco, R. D. Jeffries, F. Damiani, V. Roccatagliata, D. Fedele, and S. Randich, *Astron. Astrophys.* 616, 12 (2018).
22. R. de Grijs and G. Bono, *Astrophys. J. Suppl. Ser.* 232, 22 (2017).
23. N. V. Kharchenko, A. E. Piskunov, E. Schilbach, S. Röser, and R.-D. Scholz, *Astron. Astrophys.* 558, 53 (2013).
24. M. Kounkel, K. Covey, G. Suárez, C. Roman-Zuñiga, J. Hernandez, K. Stassun, K. O. Jaehnig, E. D. Feigelson, et al., *Astron. J.* 156, 84 (2018).
25. M. A. Kuhn, L. A. Hillenbrand, A. Sills, E. D. Feigelson, and K. V. Getman, *Astrophys. J.* 870, 32 (2019).
26. C. C. Lin and F. H. Shu, *Astrophys. J.* 140, 646 (1964).
27. L. Lindegren, J. Hernandez, A. Bombrun, S. Klioner, U. Bastian, M. Ramos-Lerate, A. de Torres, H. Steidelmüller, et al. (Gaia Collab.), *Astron. Astrophys.* 616, 2 (2018).
28. J. C. Mermilliod, M. Mayor, and S. Udry, *Astron. Astrophys.* 485, 303 (2008).
29. M. H. Pinsonneault, Y. P. Elsworth, J. Tayar, A. Serenelli, D. Stello, J. Zinn, S. Mathur, R. Garcia, et al., *Astrophys. J. Suppl. Ser.* **239**, 32 (2018).
30. A. S. Rastorguev, M. V. Zabolotskikh, A. K. Dambis, N. D. Utkin, V. V. Bobylev, and A. T. Bajkova, *Astrophys. Bull.* 72, 122 (2017).
31. A. G. Riess, S. Casertano, W. Yuan, L. Macri, B. Bucciarelli, M. G. Lattanzi, J. W. MacKenty, J. B. Bowers, et al., *Astrophys. J.* 861, 126 (2018).
32. V. Roccatagliata, G. G. Sacco, E. Franciosini, and S. Randich, *Astron. Astrophys.* 617, L4 (2018).
33. S. Röser, M. Demleitner, and E. Schilbach, *Astron. J.* 139, 2440 (2010).
34. C. Soubiran, T. Cantat-Gaudin, M. Romero-Gomez, L. Casamiquela, C. Jordi, A. Vallenari, T. Antoja, L. Balaguer-Nuñez, et al., *Astron. Astrophys.* **619**, 155 (2018).
35. K. G. Stassun and G. Torres, *Astrophys. J.* 862, 61 (2018).
36. J. P. Vallée, *Astrophys. Space Sci.* 362, 79 (2017a).
37. J. P. Vallée, *New Astron. Rev.* 79, 49 (2017b).
38. Y. Xu, S. B. Bian, M. J. Reid, J. J. Li, B. Zhang, Q. Z. Yan, T. M. Dame, K. M. Menten, et al., *Astron. Astrophys.* 616, L15 (2018).
39. L. N. Yalyalieva, A. A. Chemel', E. V. Glushkova, A. K. Dambis, and A. D. Klinichev, *Astrophys. Bull.* 73, 335 (2018).
40. E. Zari, H. Hashemi, A. G. A. Brown, K. Jardine, and P. T. de Zeeuw, *Astron. Astrophys.* **620**, 172 (2018).
41. J. C. Zinn, M. H. Pinsonneault, D. Huber, and D. Stello, arXiv: 1805.02650 (2018).